Optical and Quantum Electronics **19** *(1987) 327–349*

S_0–S_1 two photon absorption dynamics of organic dye solutions

A. PENZKOFER, W. LEUPACHER
Naturwissenschaftliche Fakultät II – Physik, Universität Regensburg, D-8400 Regensburg, FRG

Received 11 May; accepted 12 June 1987

The two-photon absorption cross-sections and excited-state absorption cross-sections of the dyes rhodamine 6G, methylene blue and fuchsin dissolved in methanol, and of the dyes safranine T, 1,3,3,1′,3′,3′-hexamethylindocarbocyanine iodide (HMICI) and 1,3,1′,3′-tetramethyl-2,2′-dioxopyrimidi-6,6′-carbocyanine hydrogen sulphate (PYC) dissolved in hexafluoroisopropanol (HFIP) are determined. The excitation is achieved with picosecond light pulses of a passively mode-locked Nd-glass laser (λ_L = 1.054 μm). The influence of amplified spontaneous emission on the two-photon absorption dynamics is analysed.

1. Introduction

The two-photon absorption in dye solutions becomes relevant at elevated laser intensities as they are readily available from Q-switched or mode-locked lasers. The two-photon absorption in dye solutions is applied for the duration measurement of picosecond laser pulses by fluorescence trace analysis [1]. Dye laser action was achieved by two-photon excitation [2, 3]. The two-photon absorption may act as a power limiter in high-power lasers [4–6]. It is a competitive third-order non-linear optical process that influences other non-linear optical effects [7].

The two-photon absorption cross-sections of dye molecules were measured previously by fluorescence analysis [9–15]. In a recent paper [16] the S_0–S_n ($n \geqslant 2$) two-photon absorption dynamics of rhodamine dyes was studied by transmission measurements and theoretical simulations.

In the present paper the S_0–S_1 two-photon absorption dynamics of the cationic dyes rhodamine 6G (a xanthene dye), safranine T (a diazine dye), methylene blue (a diazine dye), fuchsin (a triarylmethane dye), 1,3,3,1′,3′,3′-hexamethylindocarbocyanine iodide (HMICI (a cyanine dye)) and 1,3,1′,3′-tetramethyl-2,2′-dioxopyrimido-6,6′-carbocyanine hydrogen sulphate (PYC (a cyanine dye)) is studied. A mode-locked Nd-phosphate glass laser is used as pump laser (wavelength λ_L = 1.054 μm, pulse duration $\Delta t_L \approx$ 5 ps FWHM). The intensity-dependent transmission of the picosecond laser pulses is measured. The two-photon absorption cross-sections, $\sigma^{(2)}$, and excited-state absorption cross-sections, σ_{ex}^{L}, are determined by comparing the measured transmissions with computer simulations. Ground-state depletion and amplified spontaneous emission effects are discussed.

The dyes have been selected since their S_0–S_1 absorption bands are at the right wavelength region for two-photon absorption of the pump pulses and since they are potential candidates for efficient third harmonic generation of the applied pump laser [8, 33] (weak absorption) at third harmonic frequency, two-photon absorption data are necessary for analysis of third harmonic generation process).

2. Theory

A realistic level diagram for the S_0–S_1 two-photon absorption dynamics is shown in Fig. 1. The two-photon absorption process excites molecules from the S_0 ground state (region 1) to the

0306-8919/87 $03.00 + .12

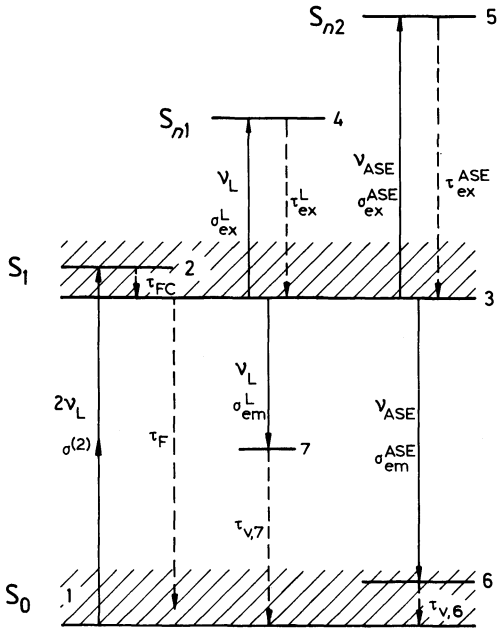

Figure 1 Level diagram.

Franck–Condon level 2 in the first excited singlet band S_1. From level 3 the molecules return to the ground state by spontaneous emission and radiationless transition (time constant τ_F) and by amplified spontaneous emission (transition to level 6). The return to the S_0-band via level 7 by stimulated emission at pump laser frequency ν_L is included. The pump laser at frequency ν_L and the generated amplified spontaneous emission signal at frequency ν_{ASE} may suffer excited-state absorption from S_1 to S_{n1} and S_{n2}, respectively. The intersystem crossing from singlet states to triplet states is neglected since the transmission behaviour of picosecond pulses is studied.

The two-photon absorption dynamics of the level system of Fig. 1 is described by the following equation system. Only isotropic single photon and two-photon absorption cross-sections are considered. The equations are transformed to a moving frame by $t' = t - nz/c_0$ where t is the time, z the spatial position in propagation direction, n the refractive index and c_0 the speed of light *in vacuo*. The equations are

$$\frac{\partial N_1}{\partial t'} = -\frac{\sigma^{(2)}(N_1 - N_2)}{2(h\nu_L)^2} I_L^2 + \sum_{i=1}^{m} (N_3 - N_{6,i}) \frac{\sigma^{ASE}_{em,i} I_{ASE,i}}{h\nu_{ASE,i}} + (N_3 - N_7) \frac{\sigma^L_{em} I_L}{h\nu_L} + \frac{N_3}{\tau_F} \tag{1}$$

$$\frac{\partial N_2}{\partial t'} = \frac{\sigma^{(2)}(N_1 - N_2)}{2(h\nu_L)^2} I_L^2 - \left(N_2 - N_4 \frac{N_2}{N_2 + N_3}\right) \frac{\sigma^L_{ex} I_L}{h\nu_L} - \frac{N_2}{\tau_{FC}} - \frac{N_2}{\tau_F} \tag{2}$$

$$\frac{\partial N_3}{\partial t'} = \frac{N_2}{\tau_{FC}} - \left(N_3 - N_4 \frac{N_3}{N_2 + N_3}\right) \frac{\sigma^L_{ex} I_L}{h\nu_L} - (N_3 - N_5) \frac{\sigma^{ASE}_{ex} I_{ASE}}{h\nu_{ASE}} - \sum_{i=1}^{m} (N_3 - N_{6,i}) \frac{\sigma^{ASE}_{em,i} I_{ASE,i}}{h\nu_{ASE,i}} - (N_3 - N_7) \frac{\sigma^L_{em} I_L}{h\nu_L} - \frac{N_3}{\tau_F} + \frac{N_4}{\tau^L_{ex}} + \frac{N_5}{\tau^{ASE}_{ex}} \tag{3}$$

$$\frac{\partial N_4}{\partial t'} = (N_2 + N_3 - N_4) \frac{\sigma^L_{ex} I_L}{h\nu_L} - \frac{N_4}{\tau^L_{ex}} \tag{4}$$

$$\frac{\partial N_5}{\partial t'} = (N_3 - N_5) \frac{\sigma^{ASE}_{ex} I_{ASE}}{h\nu_{ASE}} - \frac{N_5}{\tau^{ASE}_{ex}} \tag{5}$$

$$\frac{\partial N_{6,i}}{\partial t'} = \frac{N_3}{\tau_{rad}} e_{ASE,i} + (N_3 - N_{6,i}) \frac{\sigma^{ASE}_{em,i} I_{ASE,i}}{h\nu_{ASE,i}} - \frac{N_{6,i} - \varrho_{6,i} N_1}{\tau_{v,6}} \tag{6}$$

$$\frac{\partial N_7}{\partial t'} = (N_3 - N_7) \frac{\sigma^{L}_{em} I_L}{h\nu_L} - \frac{N_7 - \varrho_7 N_1}{\tau_{v,7}} \tag{7}$$

$$\frac{\partial I_L}{\partial z} = -\alpha_L I_L - (N_1 - N_2) \frac{\sigma^{(2)} I_L^2}{h\nu_L} - (N_2 + N_3 - N_4)\sigma^{L}_{ex} I_L + (N_3 - N_7)\sigma^{L}_{em} I_L \tag{8}$$

$$\frac{\partial I_{ASE,i}}{\partial z} = e_{ASE,i} \frac{N_3}{\tau_{rad}} h\nu_{ASE,i} \frac{\Delta\Omega}{4\pi} + (N_3 - N_{6,i})\, \sigma^{ASE}_{em,i} I_{ASE,i} - (N_3 - N_5)\sigma^{ASE}_{ex} I_{ASE,i} \tag{9}$$

The initial conditions for the number densities of the level populations (dimension cm^{-3}) are $N_1(t' = -\infty, r, z) = N_0$, $N_2(-\infty) = N_3(-\infty) = N_4(-\infty) = N_5(-\infty) = 0$, $N_{6,i}(-\infty) = \varrho_{6,i} N_0$ and $N_7(-\infty) = \varrho_7 N_0$. N_0 is the total number density of dye molecules. The amplification of spontaneous emission may occur over a wide frequently region. Within this region the stimulated emission cross-section and the terminal level population varies. In the calculations band 6 is grouped into m sublevels i of spectral width $\Delta\nu_{6,i}$. The thermal occupation factor of sublevel (6, i) is denoted $\varrho_{6,i}$. It is approximately given by $\varrho_{6,i} \approx \sigma_A(\nu_{ASE,i})/\sigma^{ASE}_{em,i}$. $\sigma^{ASE}_{em,i}$ is the stimulated emission cross-section at frequency $\nu_{ASE,i}$. $\sigma_A(\nu_{ASE,i})$ is the effective absorption cross-section at $\nu_{ASE,i}$ [17, 18]. The thermal occupation factor ϱ_7 is approximately given by $\varrho_7 \approx \sigma_A(\nu_L)/\sigma^{L}_{em}$.

The inititial light intensities are $I_L(t', r, z = 0) = I_{OL} s_t(t/t_0) s_r(r/r_0)$ and $I_{ASE,i}(t', r, z = 0) = 0$ ($i = 1, \ldots, m$). I_{OL} is the peak intensity of the pump laser light at the entrance position of the two-photon absorber. The temporal and spatial pulse shapes are assumed to be Gaussian, i.e. $s_t(t'/t_0) = \exp(-t'^2/t_0^2)$ and $s_r(r/r_0) = \exp(-r^2/r_0^2)$. t_0 is half the $1/e$-pulse width (the FWHM pulse duration is $\Delta t_L = 2[\ln(2)]^{1/2} t_0$) and r_0 is the $1/e$ beam radius of the pump pulse.

Equation 1 describes the population changes of the S_0-band. N_1 comprises the total population of the S_0 band (includes levels 6 and 7). The first term of Equation 1 is responsible for two-photon absorption. $\sigma^{(2)}$ is the orientation-averaged two-photon absorption cross-section. The second term handles the amplified spontaneous emission. The third term is due to stimulated emission at the laser frequency ν_L. The last term gives the S_1–S_0 relaxation. $\tau_F = q_F \tau_{rad}$ is the fluorescence lifteime, q_F is the fluorescence quantum efficiency and τ_{rad} is the radiative lifetime. A single exponential relaxation is assumed in the analysis.

The second equation contains the two-photon absorption, the excited-state absorption, the relaxation within the S_1-band and the S_1–S_0 relaxation. Equation 3 describes the S_1-state dynamics. The first term gives the level population by Franck–Condon relaxation. The second and third terms take care of excited-state absorption of light at frequencies ν_L and ν_{ASE}. The fourth term is due to amplified spontaneous emission, and the fifth term is due to stimulated emission at frequency ν_L. The last three terms are responsible for relaxation.

Equations 4 and 5 describe the excited-state absorptions. Equations 6 handle the populations of the sublevels (6, i) by amplified spontaneous emission. The first term gives the contribution of spontaneous emission to the frequency interval $\Delta\nu_{6,i}$. $e_{ASE,i} = E(\nu_{ASE,i})\Delta\nu_{6,i}/q_F$ is the fraction of fluorescence light which is emitted in the frequency interval $\Delta\nu_{6,i}$ around the frequency $\nu_{ASE,i}$. $E(\nu_{ASE,i})$ is the fluorescence quantum distribution ($\int_{em} E(\nu)d\nu = q_F$, integration over S_0–S_1 fluorescence band). The second term of Equation 6 gives the light amplification. The last term causes thermalization within the S_0-band with a time constant $\tau_{v,6}$.

Equation 7 represents the population of level 7 by stimulated emission of laser light at frequency ν_L. The first term gives the stimulated emission and the second term is responsible for thermalization with a time constant $\tau_{v,7}$.

The change of pump laser intensity is described by Equation 8. The first term takes linear losses into account (no transition shown in the level diagram of Fig. 1) as light scattering, vibrational

overtone absorption of solvent and impurity absorption. α_L is the linear loss coefficient. Absorption bleaching is not included in the analysis. A bleaching of α_L would lead to enlarged $\sigma^{(2)}$ and σ_{ex}^L-values in the fitting of the calculations to the measured energy transmission. The second term gives the loss of laser light due to two-photon absorption. The third term takes care of excited-state absorption, and the last term considers stimulated emission.

Equations 9 describe the amplification of fluorescence light. The first term gives the seeding spontaneous emission in a frequency interval $\Delta\nu_{6,i}$ around $\nu_{ASE,i}$. $\Delta\Omega$ is the solid angle of efficient amplified spontaneous emission. The second term causes amplification of fluorescence light and the third term described excited-state absorption. The total amplified spontaneous emission intensity I_{ASE} is given by $I_{ASE} = \Sigma_{i=1}^{m} I_{ASE,i}$.

The intensity transmission T_I is

$$T_I(t', r) = \frac{I_L(t', r, l)}{I_L(t', r, 0)} \tag{10}$$

The time-integrated intensity transmission is

$$T_{TI}(r) = \frac{\int_{-\infty}^{\infty} T_I(t', r) s(t'/t_0)\, dt'}{\int_{-\infty}^{\infty} s(t'/t_0)\, dt'} \tag{11}$$

Finally, the energy transmission $T_E = W(l)/W(0)$ (W is laser energy) is given by

$$T_E = \frac{\int_0^{\infty} T_{TI}(r) r s(r/r_0)\, dr}{\int_0^{\infty} r s(r/r_0)\, dr} \tag{12}$$

The measured energy transmission $T_{E,m}$ is related to Equation 12 by

$$T_{E,m} = \frac{W_{out}}{W_{in}} = \frac{(1 - R)W(l)}{W(0)/(1 - R)} = (1 - R)^2 T_E \tag{13}$$

R is the reflectivity of the dye cell.

The equation system 1–9 is solved numerically to determine the two-photon absorption cross-section $\sigma^{(2)}$ and the excited-state absorption cross-section σ_{ex}^L by fitting the calculated energy transmission to the measured energy transmission.

The influence of σ_{em}^L on the two-photon absorption dynamics is seen by inspection of Equation 8. Neglecting the population densities N_4 and N_7 gives

$$\frac{\partial I_L}{\partial z} = -\alpha_L I_L - (N_1 - N_2)\frac{\sigma^{(2)} I_L^2}{h\nu_L} - N_3(\sigma_{ex}^L - \sigma_{em}^L) I_L \tag{14}$$

For all investigated dyes in this paper it is $\sigma_{em}^L \ll \sigma_{ex}^L$ and the stimulated emission at the pump laser frequency ν_L has no influence on the absorption dynamics. (For the situation of $\sigma_{em}^L > \sigma_{ex}^L$ see [16].)

An estimate of the S_1-state level population is found by approximate solution of Equation 3. If no amplified spontaneous emission occurs ($\sigma_{em}^{ASE} < \sigma_{ex}^{ASE}$, see Equations 9 and [16]), Equation 3 may be approximately reduced to

$$\frac{\partial N_3}{\partial t'} = \frac{\sigma^{(2)}(N_0 - N_3)}{2(h\nu_L)^2} I_L^2 - \frac{N_3}{\tau_F} \tag{15}$$

Formal integration of Equation 15 gives

$$N_3(t_0) = \frac{\sigma^{(2)}[N_0 - N_3(t_0)] I_{OL}^2 t_{eff}}{2(h\nu_L)^2} = \frac{N_0}{2(h\nu_L)^2/[\sigma^{(2)} I_{OL}^2 t_{eff}] + 1} \tag{16}$$

where t_{eff} is approximately the minimum value of Δt_L and τ_F. The S_1-state population at time $t' = t_0$ becomes equal to $N_0/2$ for a pump pulse peak intensity of

$$I_{OL} = I_s^{(2)} = \frac{2^{1/2} h\nu_L}{[\sigma^{(2)} t_{eff}]^{1/2}} \tag{17}$$

$I_s^{(2)}$ is called the two-photon absorption saturation intensity. For a typical S_0–S_1 two-photon absorption cross-section of $\sigma^{(2)} = 2 \times 10^{-49}\,cm^4 s$ (see results below) and $t_{eff} = \Delta t_L = 5\,ps$, the two-photon saturation intensity is $I_s^{(2)} \approx 4 \times 10^{11}\,W\,cm^{-2}$ ($\lambda_L = 1.054\,\mu m$). In the experiments the non-linear transmission measurements are carried out for $I_{OL} \ll I_s^{(2)}$ so that ground-state depletion does not influence the two-photon absorption process.

If amplified spontaneous emission occurs ($\sigma_{em}^{ASE} > \sigma_{ex}^{ASE}$), then the spontaneous emission is amplified approximately exponentially [19] with a gain factor

$$G = \frac{I_{ASE}(l)}{I_{sp}(l)} \approx \exp\{(\sigma_{em}^{ASE} - \sigma_{ex}^{ASE})N_3 - \sigma_{em}^{ASE} N_6]l\} \tag{18}$$

Amplified spontaneous emission occurs for

$$N_3 > N_{3,th} = \frac{\sigma_{em}^{ASE}}{\sigma_{em}^{ASE} - \sigma_{ex}^{ASE}} N_6 \approx \frac{\sigma_{em}^{ASE}}{\sigma_{em}^{ASE} - \sigma_{ex}^{ASE}} N_0 \varrho_6 \tag{19}$$

The corresponding threshold pump laser intensity is (solution of Equation 16)

$$I_{OL} = I_{th,L}^{ASE} = h\nu_L \left(\frac{2\sigma_{em}^{ASE} \varrho_6}{\sigma^{(2)} t_{eff}[(1 - \varrho_6)\sigma_{em}^{ASE} - \sigma_{ex}^{ASE}]} \right)^{1/2} \tag{20}$$

$I_{ASE}(l)$ approaches the pump pulse intensity I_{OL} for $G \approx \exp(20)$ and limits the S_1-level population to

$$N_3 \lesssim \frac{20 + \sigma_{em}^{ASE} N_0 \varrho_6 l}{(\sigma_{em}^{ASE} - \sigma_{ex}^{ASE})l} \tag{21}$$

The limitation of the S_1-state population hinders ground-state depletion and reduces the transmission losses due to excited state absorption.

3. Experimental

The experimental arrangement for the two-photon transmission measurements is shown in Fig. 2. A mode-locked Nd-phosphate glass-laser is used in the experiments ($\lambda_L = 1.054\,\mu m$, $\Delta t_L \approx 5\,ps$). From the pulse trains single picosecond pulses are selected with a Kerr shutter. The single pulses are increased in energy by a Nd-glass amplifier. The pulses are focused to the dye samples. The input pulse peak intensity is determined by measuring the transmission through a saturable absorber in

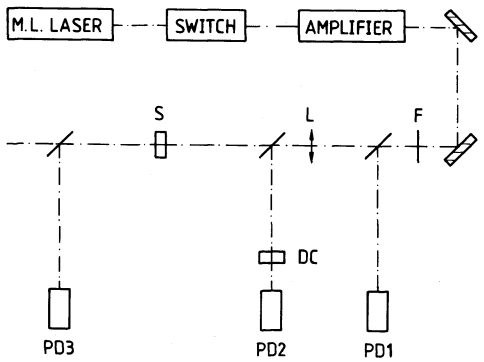

Figure 2 Experimental layout for two-photon transmission measurement. F, filter; L, lens; S, sample; DC, saturable absorber cell; PD1–PD3, photodetectors.

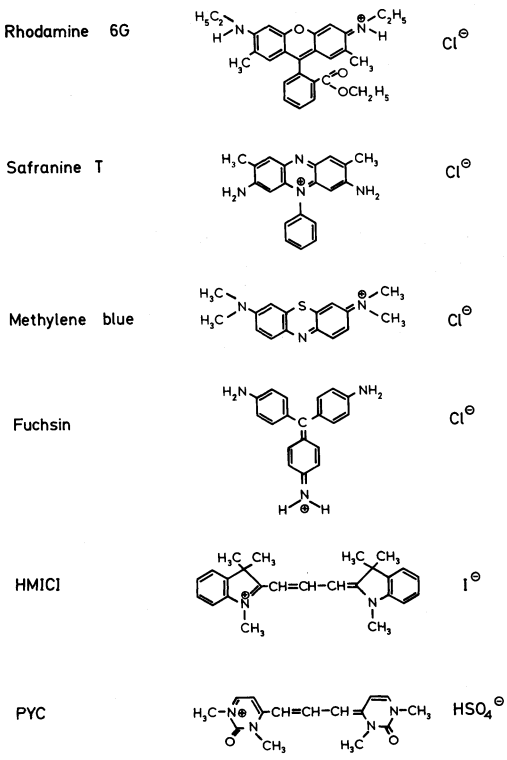

Figure 3 Structure formulae of dyes investigated. HMICI = 1,3,3,1′,3′,3′-hexamethylindocarbocyanine iodide; PYC = 1,3,1′,3′-tetramethyl-2,2′dioxopyrimidio-6,6′-carbocyanine hydrogen sulphate.

cell DC (Kodak dye No. 9860) [20] with photodetectors PD1 and PD2. The non-linear transmission through the dye sample S is measured with photodetectors PD1 and PD3. The input pulse intensities are varied by use of filters F and lenses L of different focal lengths.

Highly concentrated dye solutions have been used in the two-photos absorption measurements to achieve resonable two-photon absorption losses. At these high concentrations dye aggregation occurs [21–27]. The absorption cross-section spectra, stimulated emission cross-section spectra, and fluorescence lifetimes at high concentrations have been determined by absorption spectra [28, 29], emission spectra [29, 30] and fluorescence quantum distribution measurements [30, 31].

4. Spectroscopic properties of investigated dyes

The structural formulae of the investigated dyes are collected in Fig. 3. The dye concentrations and solvents used in the two-photon absorption measurements are listed in Table I. All dyes are used without further purification.

The monomer and dimer absorption and monomer cross-section spectra of the dyes rhodamine 6G chlorid (Kodak) and 1,3,1′,3′-tetramethyl-2,2′-dioxo-pyrimido-6,6′-carbocyanine hydrogen sulphate (PYC, gift of Dr U. Mayer, BASF, and Professor K. H. Drexhage) are given in [30] and [29], respectively. The monomer and dimer cross-section spectra of safranine T (Fluka) are presented in Fig. 4. For 1,3,3,1′,3′,3′-hexamethyl-indocarbocyanine iodide (HMICI, Koch-Light) the monomer and dimer absorption cross-section spectra are shown together with the monomer emission cross-section spectrum in Fig. 5. The dimer emission cross-section spectrum could not be resolved since excimers [32] are formed by the excitation of highly concentrated HMICI solutions. For methylene blue (Merck) and fuchsin (Fluka) only the monomer spectra have been measured and they are presented in Figs 6 and 7.

The actual cross-sections $\sigma_A(\lambda, C)$ and $\sigma_{em}(\lambda, C)$ at concentration C and wavelength

TABLE I Dye parameters. Pump laser parameters are wavelength $\lambda_L = 1.054\,\mu m$ and pulse duration $\Delta t_L = 5\,ps$ (FWHM). The meaning of many parameters is explained in Fig. 1. Assumed solid angle of amplified spontaneous emission $\Delta\Omega = 3 \times 10^{-6}\,sr$

Parameter	Transition	Rhodamine 6G	Safranine T	Methylene blue	Fuchsin	HMICI*	PYC†	Comments
Concentration C (mol dm^{-3})		0.2	0.33	0.2	0.2	0.08	0.1	
Number density N_0 (cm^{-3})		1.2×10^{20}	2×10^{20}	1.2×10^{20}	1.2×10^{20}	4.8×10^{19}	6×10^{19}	
Solvent		Methanol	HFIP‡	Methanol	Methanol	HFIP†	HFIP‡	
Sample length l(cm)		2	1	1	2	1	1	
Dimer mole fraction x_D		0.34 [28]	0.93 [29]			0.93	0.83	Fig. 9
linear loss α_L (cm^{-1})		0.195	0.277	1.32	0.764	0.181	0.071	
$\tau_{rad,M}$ (ns)	3 → 1	4.3 [30]	10	7	5.5	3.4	3.3 [29]	Eq. 26
$\tau_{rad,D}$ (ns)	3 → 1	4.6 [30]	17				4.1 [29]	Eq. 26
$\tau_{rad,eff}$ (ns)	3 → 1	4.4	16.2				3.94	Eq. 27
q_F	3 → 1	1.3×10^{-3} [30, 31]	7.4×10^{-3}			2.7×10^{-2}	2.4×10^{-3} [29]	Fig. 12
τ_F (ps)	3 → 1	8 [31]	120			92	9.5 [29]	Eq. 29
τ_{FC} (ps)	2 → 3	0.7 [41]	0.7			0.7	0.7	Assumed
τ_{ex}^{L} (ps)	4 → 3	0.1 [19, 42]	0.1			0.1	0.1	Assumed
τ_{ex}^{ASE} (ps)	5 → 3	0.1	0.1			0.1	0.1	Assumed
$\tau_{v,6}$ (ps)	6 → 1	4 [43]	4			4	4	Assumed
$\tau_{v,7}$ (ps)	7 → 1	0.1	0.1			0.1	0.1	Assumed
σ_{em}^{L} (cm^2)	3 → 7	$\sim 10^{-21}$	$\sim 2 \times 10^{-19}$			$\sim 1.5 \times 10^{-19}$	$\sim 7 \times 10^{-20}$	Extrapolated
σ_{ex}^{ASE} (cm^2)	3 → 6	0	0			0	0	Assumed§
σ_{ex}^{L} (cm^2)	3 → 4	$(2.5 \pm 1) \times 10^{-17}$ [44]	$(7 \pm 3) \times 10^{-18}$	$(2 \pm 1) \times 10^{-17}$	$(4 \pm 2) \times 10^{-17}$	$(2 \pm 0.5) \times 10^{-17}$	$\leqslant 3 \times 10^{-18}$	
$\sigma^{(2)}$ (cm^4 s)	1 → 2	$(1 \pm 0.1) \times 10^{-49}$	$(5 \pm 1) \times 10^{-50}$	$(7 \pm 1) \times 10^{-50}$	$(1 \pm 0.1) \times 10^{-49}$	$(2 \pm 0.2) \times 10^{-49}$	$(1.8 \pm 0.2) \times 10^{-49}$	
$I_s^{(2)}$ (W cm^{-2})		4.5×10^{11}	5.3×10^{11}	4.5×10^{11}	3.8×10^{11}	2.7×10^{11}	2.8×10^{11}	Eq. 17
$I_{th,L}^{ASE}$ (W cm^{-2})		1×10^{10}	2.5×10^{10}			2×10^{10}	7×10^{9}	Eq. 20, Figs 14, 16, 20, 22

*HMICI = 1,3,3,1′,3′,3′-hexamethylindocarbocyanine iodide.
†PYC = 1,3,1′,3′-tetramethyl-2,2′-dioxopyrimido-6,6′-carbocyanine hydrogen sulphate.
‡HFIP = hexafluoroisopropanol $(CF_3)_2CHOH$.
§$\sigma_{em}^{ASE} - \sigma_{ex}^{ASE}$ determines amplification of spontaneous emission (see Fig. 26).

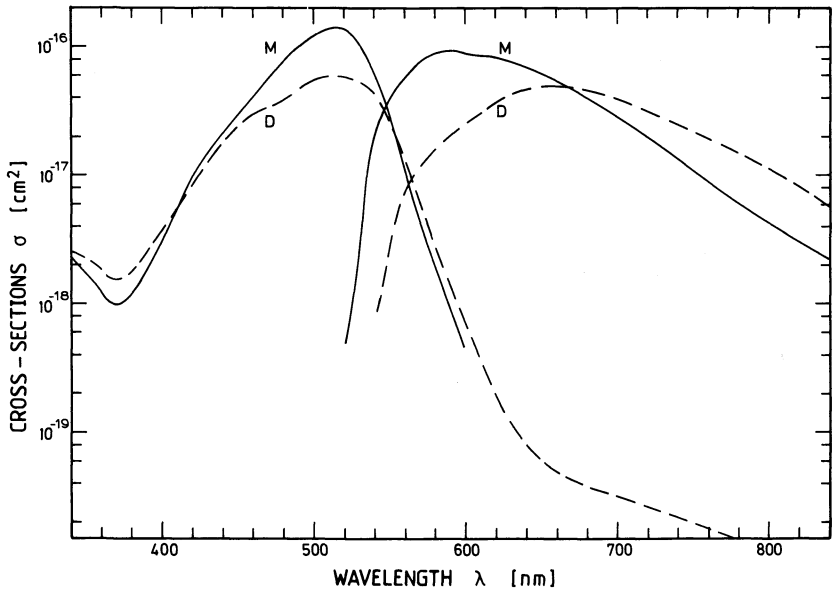

Figure 4 Absorption and emission cross-section spectra of monomers (M) and closely-spaced pairs (D) of Safranine T dissolved in hexafluoroisopropanol. The S_0–S_1 cross-section integrals are $\int_{abs}\sigma_{A,M}(\tilde{\nu})d\tilde{\nu} = 4 \times 10^{-13}$ cm, $\int_{abs}\sigma_{A,D}(\tilde{\nu})d\tilde{\nu} = 2.25 \times 10^{-13}$ cm, $\int_{em}\sigma_{em,M}(\tilde{\nu})d\tilde{\nu} = 3.05 \times 10^{-13}$ cm and $\int_{em}\sigma_{em,D}(\tilde{\nu})d\tilde{\nu} = 1.7 \times 10^{-13}$ cm.

$\lambda(\lambda = c_0/\nu = \tilde{\nu}^{-1})$ are calculated from the monomer and dimer spectra by the relation [33]

$$\sigma_i(\lambda, C) = (1 - x_D)\theta\sigma_{i,M}(\lambda) + x_D\sigma_{i,D}(\lambda), \quad i = A, em \tag{22}$$

x_D is the mole fraction of molecules in dimers or closely spaced pairs. For the dyes rhodamine 6G [28] and PYC [29] x_D has been determined previously. For the dyes safranine T and HMICI, x_D is

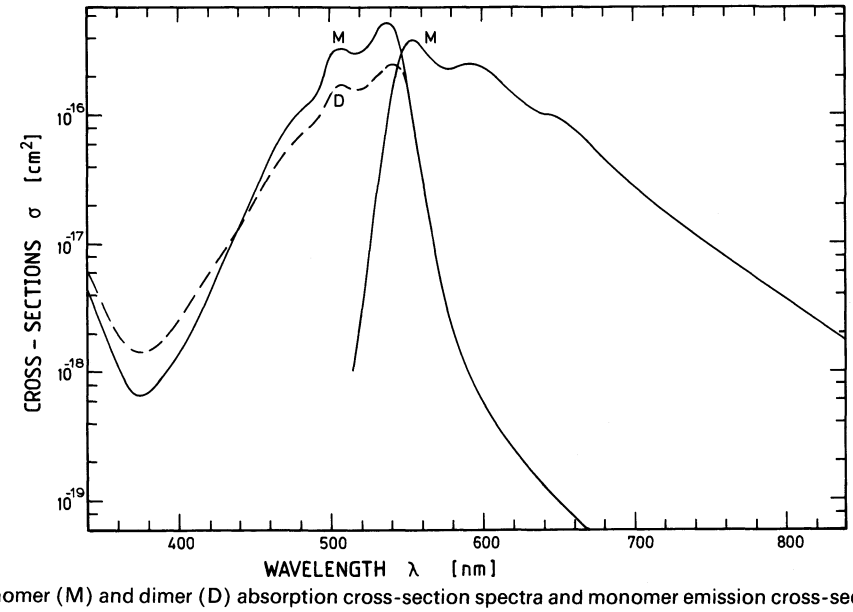

Figure 5 Monomer (M) and dimer (D) absorption cross-section spectra and monomer emission cross-section spectrum of 1,3,3,1',3',3'-hexamethylindocarbocyanine iodide (HMICI) dissolved in hexafluoroisopropanol (HFIP). The S_0–S_1 cross-section integrals are $\int_{abs}\sigma_{A,M}(\tilde{\nu})d\tilde{\nu} = 9.75 \times 10^{-13}$ cm, $\int_{abs}\sigma_{A,D}(\tilde{\nu})d\tilde{\nu} \approx 5.6 \times 10^{-13}$ cm, and $\int_{em}\sigma_{em,M}(\tilde{\nu})d\tilde{\nu} = 8.3 \times 10^{-13}$ cm.

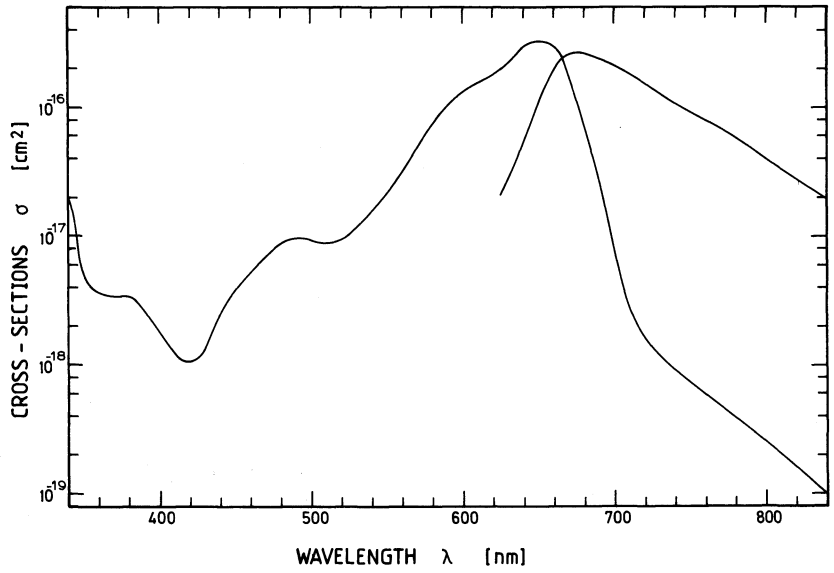

Figure 6 Absorption and emission cross-section spectra of monomers of methylene blue dissolved in methanol.

determined here from the concentration dependence of σ_A at the wavelength of maximum S_0–S_1 absorption (Equation 22). The fraction of molecules, x_D, in closely spaced pairs is given by [21, 28]

$$x_D = 1 - \exp(-V_1 N_A C) \tag{23}$$

V_1 is the interaction volume of a closely spaced pair, N_A is the Avogadro number. V_1 is determined by the best fit of Equation 22 to the experimental absorption cross-sections ($\sigma_{A,M}$ is the absorption cross-section of highly diluted solution). The experimental data of $\sigma_A(\lambda_{max}, C)/\sigma_{A,M}(\lambda_{max})$ and the best-fit curves are shown in Fig. 8 for safranine T and HMICI.

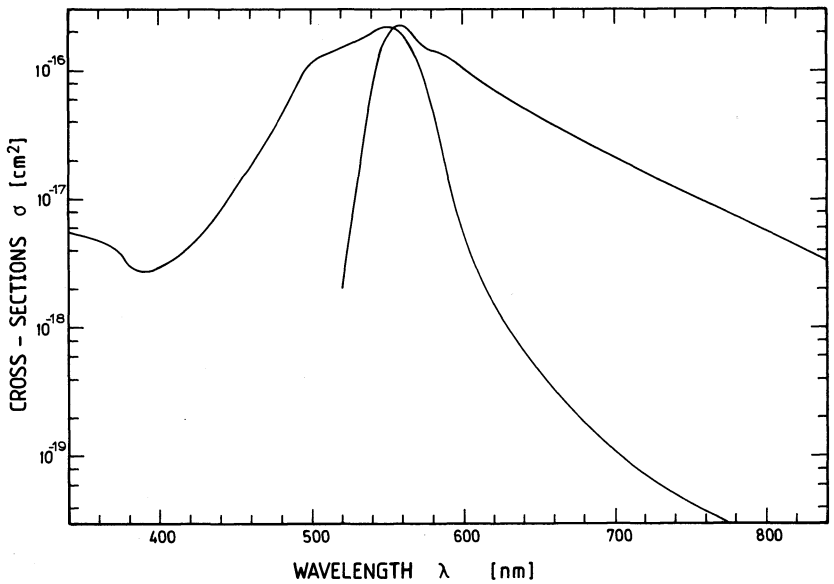

Figure 7 Absorption and emission cross-section spectra of monomers of fuchsin dissolved in methanol. The S_0–S_1 cross-section integrals are $\int_{abs}\sigma_{A,M}(\tilde{\nu})d\tilde{\nu} = 5.8 \times 10^{-13}$ cm and $\int_{em}\sigma_{em,M}(\tilde{\nu})d\tilde{\nu} = 5.1 \times 10^{-13}$ cm.

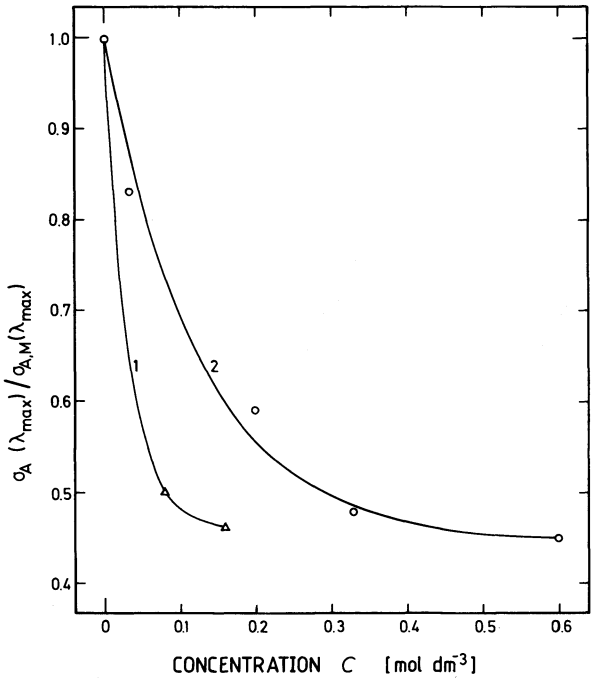

Figure 8 Determination of closely spaced pair parameters from concentration-dependent absorption cross-section measurements. Curve 1 and triangles (Δ): HMICI in HFIP. λ_{max} = 538 nm. Parameters of Equations 22 and 23 are $\sigma_{A,D}/\sigma_{A,M}$ = 0.46 and V_1 = 55 nm^3. Curve 2 and circles (○): safranine T dissolved in HFIP. λ_{max} = 516 nm, $\sigma_{A,D}/\sigma_{A,M}$ = 0.449, V_1 = 13.3 nm^3.

Knowing V_1, x_D is obtained by application of Equation 23. For the dyes rhodamine 6G, PYC, safranine T and HMICI the dependence of x_D on the concentration C is depicted in Fig. 9.

The fluorescence quantum distribution, $E(\lambda, C)$, of the dyes rhodamine 6G [30] and PYC [29] have been determined previously. $E(\lambda, C)$-curves of the dyes safranine T and HMICI are presented in Figs 10 and 11, respectively. In case of safranine T, curve 1 ($C = 10^{-3}$ mol dm^{-3}, same curve is

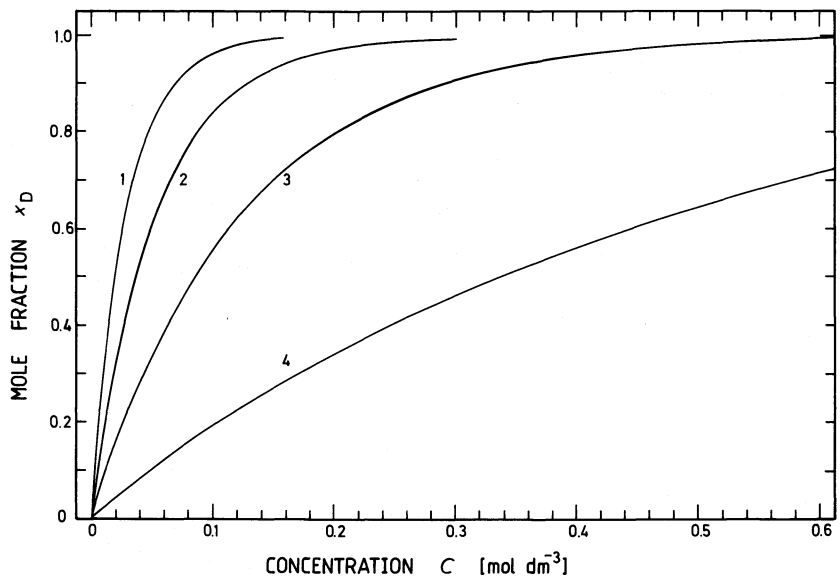

Figure 9 Fraction of dye molecules in closely spaced pairs versus concentration. Curves 1, HMICI in HFIP; 2, PYC in HFIP; 3 safranine T in HFIP; 4, rhodamine 6G in methanol.

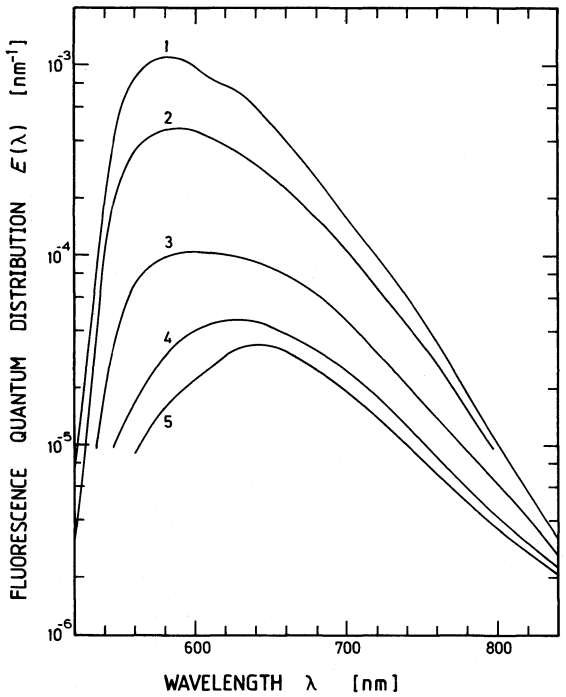

Figure 10 Fluorescence quantum distributions of safranine T in HFIP for various concentrations. Curves 1, $C = 10^{-3}$ mol dm^{-3}, resembles monomer quantum distribution, same curve is obtained for $C = 10^{-5}$ mol dm^{-3}; 2, $C = 0.031$ mol dm^{-3}; 3, $C = 0.125$ mol dm^{-3}; 4 $C = 0.33$ mol dm^{-3}; 5, $C = 0.6$ mol dm^{-3}, resembles closely spaced pair quantum distribution.

obtained for $C = 10^{-5}$ mol dm^{-3}) represents the monomer fluorescence quantum distribution $E_M(\lambda)$, and curve 5 ($C = 0.6$ mol dm^{-3}, $x_D \approx 0.99$) represents the dimer fluorescence quantum distribution $E_D(\lambda)$.

The fluorescence quantum distribution spectra of fresh solutions of HMICI in hexafluoro-isopropanol exhibit excimer formation at high concentrations (curves 2′ and 3′ in Fig. 11). In old

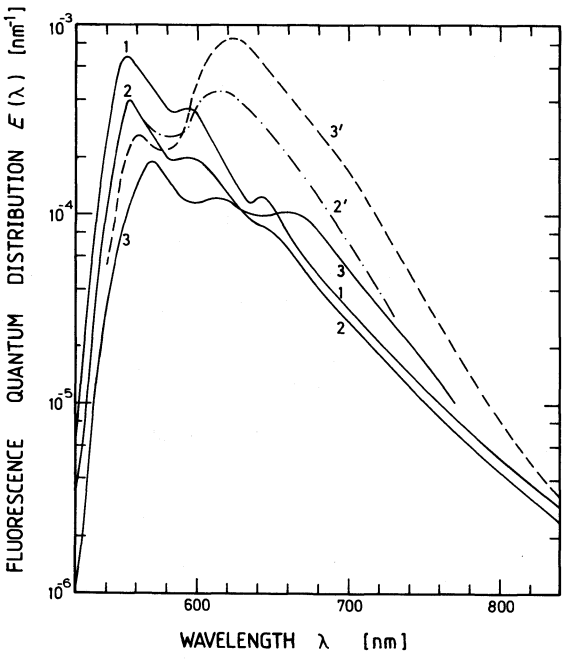

Figure 11 Fluorescence quantum distributions of HMICI in HFIP. Curves 1, concentration $C = 10^{-5}$ mol dm^{-3}, fresh and old solution (resembles monomer quantum distribution); 2, $C = 0.08$ mol dm^{-3} old solution; 2′, $C = 0.08$ mol dm^{-3} fresh solution; 3, $C = 0.16$ mol dm^{-3} old solution; 3′, $C = 0.16$ mol dm^{-3} fresh solution (excimer formation).

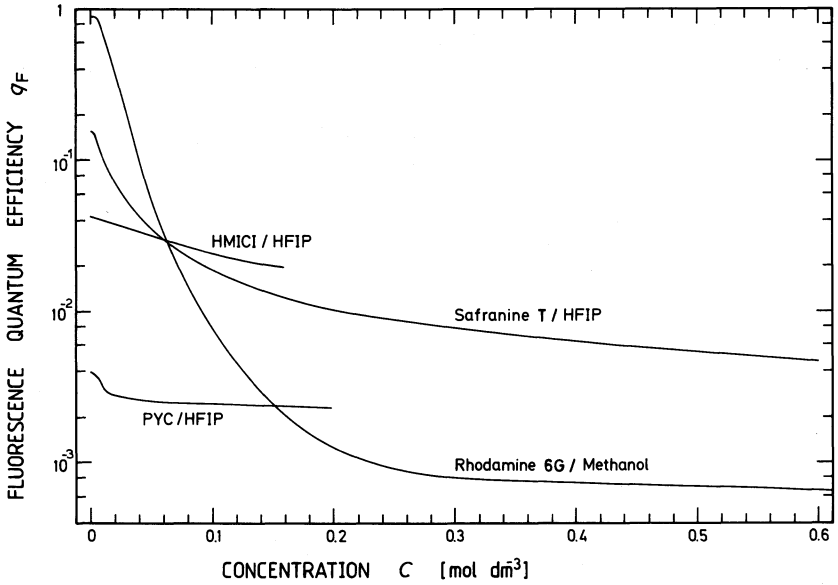

Figure 12 Fluorescence quantum efficiencies.

HMICI-hexafluoroisopropanol solutions (some days old) the tendency of excimer formation is greatly reduced (curve 3). For HMICI-methanol solutions the tendency of excimer formation does not diminish with the age of the solution.

The fluorescence quantum efficiencies, $q_F(C)$, are obtained from the fluorescence quantum distributions, $E(\lambda, C)$, by the relation

$$g_F(C) = \int_{em} E(\lambda, C)\, d\lambda \tag{24}$$

The integration extends over the S_1–S_0 emission band. For the dyes rhodamine 6G, safranine T and HMICI (old solution) the fluorescence quantum efficiency versus concentration is depicted in Fig. 12.

The radiative lifetimes of the monomers, $\tau_{rad,M}$, and of the dimers, $\tau_{rad,D}$, may be calculated by use of the Strickler–Berg formula [34, 35]

$$\frac{1}{\tau_{rad,i}} = \frac{8\pi n_F^3 c_0}{n_A} \frac{\int_{em} E_i(\lambda)\lambda d\lambda}{\int_{em} E_i(\lambda)\lambda^4 d\lambda} \int_{abs} \frac{\sigma_{A,i}(\lambda)}{\lambda}\, d\lambda \tag{25}$$

n_A and n_F are the average refractive indices of the solution in the S_0–S_1 absorption band and S_1–S_0 fluorescence band, respectively. The integrations extend over the S_1–S_0 emission band (em) and the S_0–S_1 absorption band (abs). A concentration-dependent effective radiative lifetime may be defined by the relationship

$$\tau_{rad,eff}^{-1}(C) = (1 - x_D)\tau_{rad,M}^{-1} + x_D \tau_{rad,D}^{-1} \tag{26}$$

In the case of single exponential fluorescence decay the fluorescence lifetime, $\tau_{F,i} (i = M, D)$ is given

$$\tau_{F,i} = q_{F,i}\tau_{rad,i} \tag{27}$$

In the following analysis of the two-photon absorption dynamics the monomer and dimer contributions are not seperated. In this crude description the concentration-dependent fluorescence lifetime (as may be determined by streak camera measurements) may be approximated by

$$\tau_F(C) \approx q_F(C)\tau_{rad,eff}(C) \tag{28}$$

The stimulated emission cross-sections $\sigma_{em,M}$ and $\sigma_{em,D}$ are calculated by use of the relationship [36]

$$\sigma_{em,i}(\lambda) = \frac{\lambda^4 E_i(\lambda)}{8\pi n_F^2 c_0 \tau_{rad,i} q_{F,i}}, \quad i = M, D \tag{29}$$

$\sigma_{em}(\lambda, C)$ is obtained by application of Equation 22. The stimulated emission cross-sections $\sigma_{em,M}(\lambda)$ and $\sigma_{em,D}(\lambda)$ of safranine T are shown in Fig. 4. $\sigma_{em,M}(\lambda)$ of HMICI is depicted in Fig. 5. $\sigma_{em,D}(\lambda)$ of HMICI cannot be calculated by use of Equation 29, because the shapes of the fluorescence spectra of highly concentrated HMICI solutions change with time due to the dynamics of excimer formation and the mirror symmetry between the absorption spectrum and the fluorescence quantum distribution spectrum is lost.

5. Two-photon absorption results

The measured two-photon transmissions T_E versus input pulse peak intensity I_{OL} are depicted in Figs 13 (rhodamine 6G), 15 (safranine T), 17 (methylene blue), 18 (fuchsin), 19 (HMICI) and 21 (PYC). The solvent absorptions are included in Fig. 13 (methanol, $\alpha_L = 0.112\,cm^{-1}$) and Fig. 21 (hexafluoroisopropanol, $\alpha_L = 0.07\,cm^{-1}$).

The curves in the figures are calculated by solving numerically the equation system 1–9. The dye parameters of Table I and of Figs 4–12 are used. The two-photon absorption cross-sections $\sigma^{(2)}$ and the excited-state absorption cross-sections σ_{ex}^L are varied. The best-fitting $\sigma^{(2)}$ and σ_{ex}^L values are included in Table I. For rhodamine 6G two-photon absorption cross-sections have been reported already (same excitation wavelength) [9–11, 37–39]. The reported results agree reasonably well with

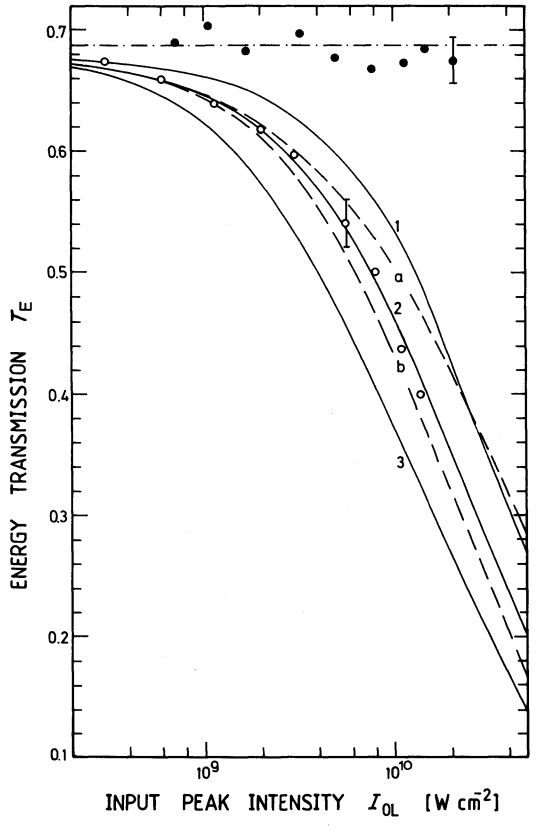

Figure 13 energy transmission versus input pulse peak intensity of rhodamine 6G dissolved in methanol. Concentration $C = 0.2\,mol\,dm^{-3}$. Sample length $l = 2\,cm$. Curves are calculated by use of data of Table I and cross-section spectra and quantum distribution spectra of [30]. 1, $\sigma^{(2)} = 5 \times 10^{-50}\,cm^4\,s$ and $\sigma_{ex}^L = 2 \times 10^{-17}\,cm^2$; 2, $\sigma^{(2)} = 1 \times 10^{-49}\,cm^4\,s$ and $\sigma_{ex}^L = 2 \times 10^{-17}\,cm^2$; 3, $\sigma^{(2)} = 2 \times 10^{-49}\,cm^4\,s$ and $\sigma_{ex}^L = 2 \times 10^{-17}\,cm^2$; a, $\sigma^{(2)} = 10^{-49}\,cm^4\,s$ and $\sigma_{ex}^L = 0$; b, $\sigma^{(2)} = 10^{-49}\,cm^4\,s$ and $\sigma_{ex}^L = 4 \times 10^{-17}\,cm^2$; σ_{em}^{ASE} does not influence the energy transmission. Chain-broken curve and closed circles represent methanol transmission.

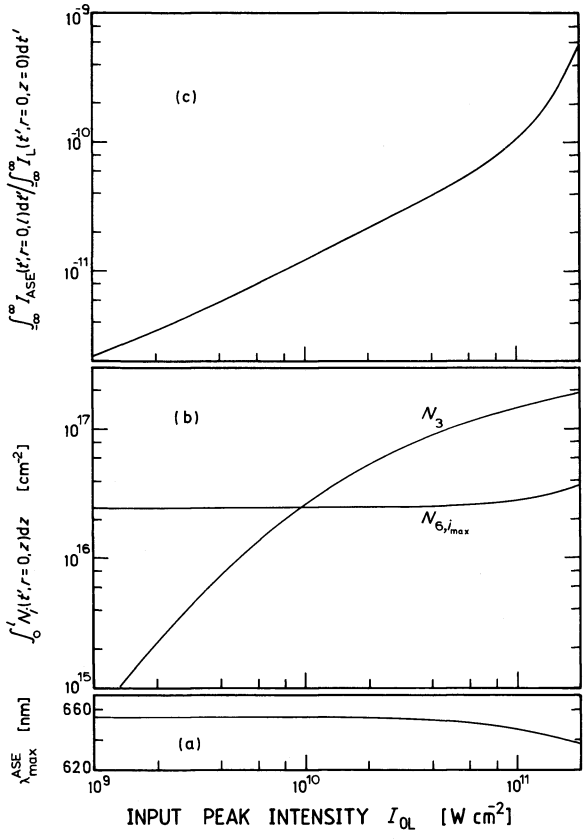

Figure 14 Characterization of two-photon induced amplified spontaneous emission of rhodamine 6G dissolved in methanol. Parameters are listed in Table I and cross-section spectra are given in [30]. $\sigma_{ex}^{ASE} = 0$ is used in calculations (overestimation of effect of amplified spontaneous emission). (a) Wavelength of amplified spontaneous emission peak. (b) Length-integrated population number densities of levels 3 (upper ASE level) and 6 (lower ASE level) at time $t' = 2.45$ ps. For comparison $\int_0^l N_0 dz = 2.4 \times 10^{20}$ cm^{-2}. (c) Normalized time-integrated ASE-signal $I_{ASE} = \Sigma_{i=1}^{m} I_{ASE,i}$.

our result of $(1 \pm 0.1) \times 10^{-49}$ cm^{4}s. For the other dyes no previously published two-photon absorption cross-sections are known.

The level populations and the build-up of amplified spontaneous emission signals are illustrated in Figs 14 (rhodamine 6G), 16 (safranine T), 20 (HMICI) and 22 (PYC). The curves are calculated with the data of Table I and Figs 4–12. The excited-state absorption of fluorescence light is neglected; that is, $\sigma_{ex}^{ASE} = 0$ is used. For all investigated dyes the ground-state depletion is negligible ($N_1 = N_0 - N_3$, $N_3 \ll N_0$ even at the highest intensities).

The wavelength of peak fluorescence emission versus pump pulse intensity is depicted in Figs 14a, 16a, 20a and 22a. With rising S_1-state level population at high pump pulse intensities the emission peak shifts to shorter wavelengths (higher stimulated emission cross-section σ_{em}^{ASE}).

The integrated level population $\int_0^l N_3(t' = 2.45\,\text{ps}, r = 0, z)dz$ and $\int_0^l N_{6,i_{max}}(t' = 2.45\,\text{ps}, r = 0, z)dz$ are plotted in Figs 14b, 16b, 20b and 22b. $N_{6,i_{max}}$ is the population number density of the lower amplified spontaneous emission level at wavelength λ_{max}^{ASE} (spectral width $\Delta\lambda_{i_{max}} = 10$ nm). The initial value is $N_{6,i_{max}}(t' = -\infty) = \varrho_{6,i_{max}} N_0 = [\sigma_A(\lambda_{max}^{ASE})/\sigma_{em}(\lambda_{max}^{ASE})]N_0$.

For $\int_0^l N_3 dz > \int_0^l N_6 dz$ amplification of spontaneous emission sets in and the amplified spontaneous emission signal rises steeply (see Figs 14c, 16c, 20c and 22c). The amplification of fluorescence light fills the lower ASE-level 6. The accumulation of population in level 6 depends on the thermalization time $\tau_{v,6}$ [16]. The shorter $\tau_{v,6}$ is, the smaller the accumulation of population in level 6 (see [16]). The influence of $\tau_{6,v}$ on N_3 and N_6 is illustrated in Fig. 22.

The S_1-state population $\int_0^l N_3 dz$ rises quadratically with intensity at low pump pulse intensities. At high pump intensities $\int_0^l N_3 dz$ levels off to a linear rise since at high input intensities nearly all pump photons are absorbed by two-photon absorption ($T_E \to 0$) and the number of excited molecules becomes proportional to the number of incident pump photons. If amplification of

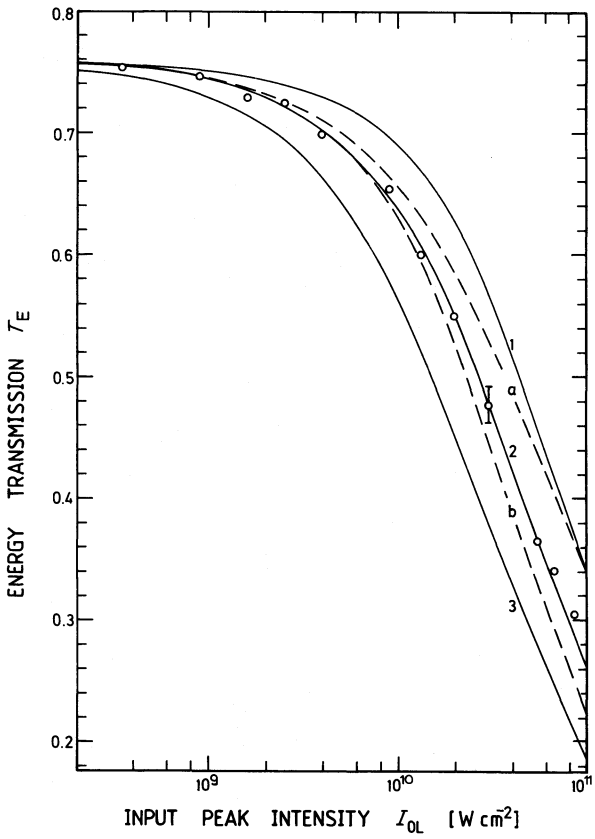

Figure 15 Energy transmission of safranine T in HFIP. Data are listed in Table I. Cross-section spectra and fluorescence quantum distribution spectra are given in Figs 4 and 10, respectively. The curves belong to: 1, $\sigma^{(2)} = 2.5 \times 10^{-50}$ cm^{4}s and $\sigma_{ex}^{L} = 5 \times 10^{-18}$ cm^2; 2, $\sigma^{(2)} = 5 \times 10^{-50}$ cm^{4}s and $\sigma_{ex}^{L} = 5 \times 10^{-18}$ cm^2; 3, $\sigma^{(2)} = 10^{-49}$ cm^{4}s and $\sigma_{ex}^{L} = 5 \times 10^{-18}$ cm^2; a, $\sigma^{(2)} = 5 \times 10^{-50}$ cm^{4}s and $\sigma_{ex}^{L} = 0$; b, $\sigma^{(2)} = 5 \times 10^{-50}$ cm^{4}s and $\sigma_{ex}^{L} = 10^{-17}$ cm^2. σ_{em}^{ASE} does not influence the energy transmission.

spontaneous emission becomes effective the rise of $\int_0^l N_3 dz$ with input pump intensity levels off further due to stimulated transitions to the lower ASE-level 6.

The efficiency of amplified spontaneous emission light generation, $\int_{-\infty}^{\infty} I_{ASE}(t', r = 0, l)dt' / \int_{-\infty}^{\infty} I_L(t', r = 0, z = 0)dt'$, is plotted in Figs 14c, 16c, 20c and 22c. The $\sigma^{(2)}$ and σ_{ex}^{L} determination is not disturbed by σ_{em}^{ASE}, since in the intensity range of experimental energy transmission measurement the amplification of spontaneous emission is still too weak to change significantly the level population N_3. The situation would be different for PYC where the level population N_3 is reduced above $I_{0L} \approx 4 \times 10^{10}$ W cm^{-2} by amplification of spontaneous emission and T_E-measurements have been carried out up to $I_{0L} \approx 8 \times 10^{10}$ W cm^{-2}. However, for this dye the excited-state absorption is negligible) $\sigma_{ex}^{L} \leqslant 3 \times 10^{-18}$ cm^2) and a reduction of N_3 has no influence on the two-photon absorption (ground state becomes not depleted).

6. Influence of various parameters

The build-up of amplified spontaneous emission and its influence on the energy transmission under various experimental conditions are shown in Figs 23 to 25. The data of 0.2 M rhodamine 6G in methanol are used. The varied parameters are listed in the figure captions.

The dependences of T_{TI}, I_{ASE}, N_3 and N_6 on the sample length are illustrated in Fig. 23. For the selected input peak intensity of $I_{0L} = 10^{11}$ W cm^{-2} the transmission decreases strongly within the first 2 mm and then levels off. Correspondingly the level population $\int_0^l N_3 dz$ increases strongly and causes a strong rise of I_{ASE} within the first 2 mm. The amplified spontaneous emission signal rises with increasing σ_{em}^{ASE}. After a steep rise of the amplified spontaneous emission intensity to a peak

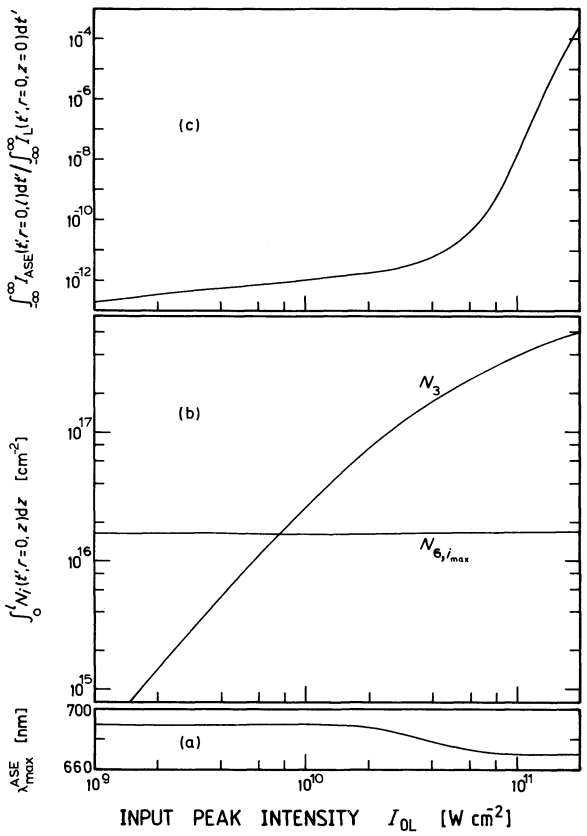

Figure 16 Characterization of two-photon induced amplified spontaneous emission of safranine T dissolved in HFIP. Parameters are listed in Table I. Cross-section spectra are shown in Fig. 4. (a) Wavelength-amplified spontaneous emission peak. (b) Length-integrated population number density of levels 3 and 6 at time $t' = 2.45$ ps. For comparison $\int_0^l N_0 dz = 2 \times 10^{20}$ cm^{-3}. (c) Time-integrated ASE signal normalized to time-integrated input pump pulse signal.

value, I_{ASE} reduces due to the linear rise of $\int_0^l N_6 dz$ with sample length while $\int_0^l N_3 dz$ remains approximately constant (pump pulse already absorbed, $I_{ASE} \propto \exp(\sigma_{em}^{ASE}\{[N_3(z) - N_6(z)]dz\})$. The occurrence of excited-state absorption reduces the efficiency of amplified spontaneous emission generation since pump photons are lost by this process (curve 4, $\sigma_{ex}^{L} = 0$; curve 1, $\sigma_{ex}^{L} = 2 \times 10^{-17}$ cm^2; other parameters are unchanged).

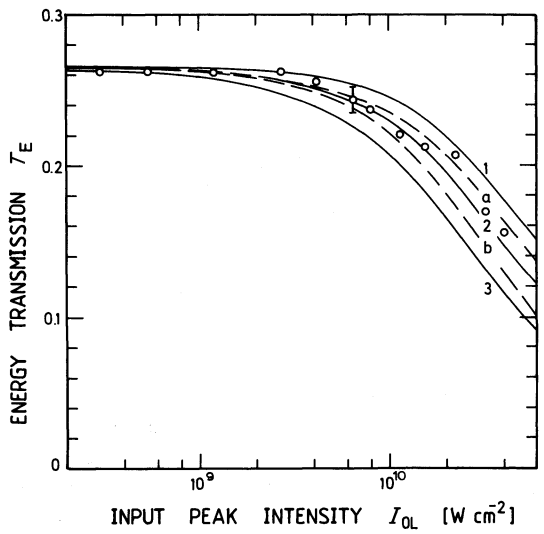

Figure 17 Energy transmission of laser light through methylene blue in methanol. Data are listed in Table I. Cross-section spectra are shown in Fig. 6 (monomer data are used). The curves belong to: 1, $\sigma^{(2)} = 4 \times 10^{-50}$ cm^{4}s and $\sigma_{ex}^{L} = 2 \times 10^{-17}$ cm^2; 2, $\sigma^{(2)} = 8 \times 10^{-50}$ cm^{4}s and $\sigma_{ex}^{L} = 2 \times 10^{-17}$ cm^2; 3, $\sigma_{ex}^{L} = 1.6 \times 10^{-49}$ cm^{4}s and $\sigma_{ex}^{L} = 2 \times 10^{-17}$ cm^2; a, $\sigma^{(2)} = 8 \times 10^{-50}$ cm^{4}s and $\sigma_{ex}^{L} = 10^{-17}$ cm^2; b, $\sigma^{(2)} = 8 \times 10^{-50}$ cm^{4}s and $\sigma_{ex}^{L} = 4 \times 10^{-17}$ cm^2. $\sigma_{em}^{ASE} = 0$ is used in the calculations.

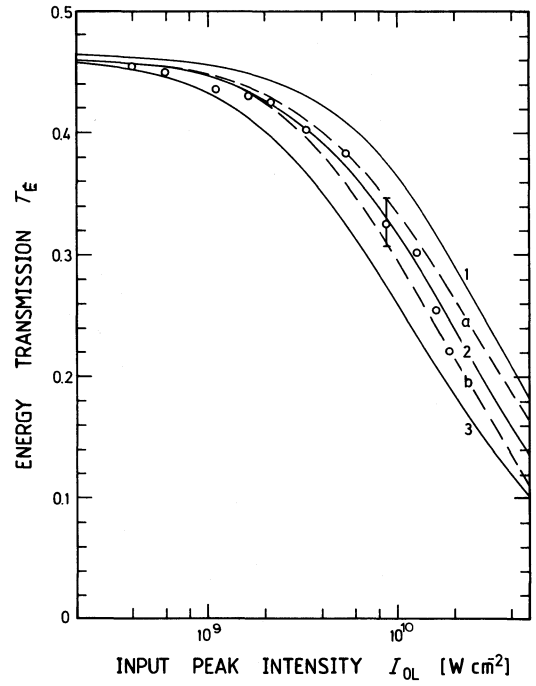

Figure 18 Energy transmission of laser light through fuchsin in methanol. Data are listed in Table I. Cross-section spectra are shown in Fig. 7 (monomer data are used). The curves belong to: 1, $\sigma^{(2)} = 5 \times 10^{-50}$ cm^4 s and $\sigma_{ex}^{L} = 4 \times 10^{-17}$ cm^2; 2, $\sigma^{(2)} = 10^{-49}$ cm^4 s and $\sigma_{ex}^{L} = 4 \times 10^{-17}$ cm^2; 3, $\sigma^{(2)} = 2 \times 10^{-49}$ cm^4 s and $\sigma_{ex}^{L} = 4 \times 10^{-17}$ cm^2; a, $\sigma^{(2)} = 10^{-49}$ cm^4 s and $\sigma_{ex}^{L} = 2 \times 10^{-17}$ cm^2; b, $\sigma^{(2)} = 10^{-49}$ cm^4 s and $\sigma_{ex}^{L} = 8 \times 10^{-17}$ cm^2. $\sigma_{em}^{ASE} = 0$ is used in the calculations.

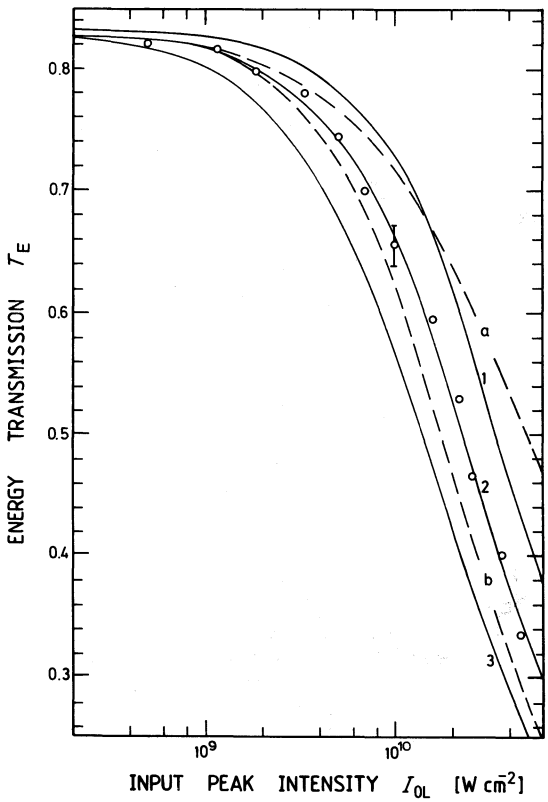

Figure 19 Energy transmission of laser light through HMICl dissolved in HFIP. Data are listed in Table I. Cross-section spectra and fluorescence quantum-distribution spectra are shown in Figs 5 and 11, respectively. The curves belong to: 1, $\sigma^{(2)} = 10^{-49}$ cm^4 s and $\sigma_{ex}^{L} = 2 \times 10^{-17}$ cm^2; 2, $\sigma^{(2)} = 2 \times 10^{-49}$ cm^4 s and $\sigma_{ex}^{L} = 2 \times 10^{-17}$ cm^2; 3, $\sigma^{(2)} = 4 \times 10^{-49}$ cm^4 s and $\sigma_{ex}^{L} = 2 \times 10^{-17}$ cm^2; a, $\sigma^{(2)} = 2 \times 10^{-49}$ cm^4 s and $\sigma_{ex}^{L} = 0$; b, $\sigma^{(2)} = 2 \times 10^{-49}$ cm^4 s and $\sigma_{ex}^{L} = 4 \times 10^{-17}$ cm^2. σ_{em}^{ASE} does not influence the energy transmission.

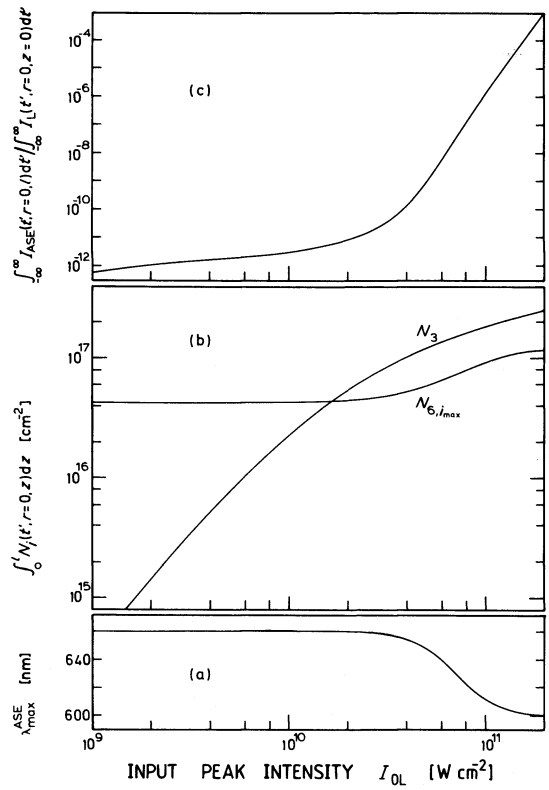

Figure 20 Characterization of two-photon induced amplified spontaneous emission of HMICl dissolved in HFIP. Parameters are listed in Table I. Cross-section spectra and fluorescence quantum distribution spectra are shown in Figs 5 and 11, respectively. Monomer data are used for σ_{em}^{ASE} and $E(\lambda)$. (a) Wavelength of peak amplified spontaneous emission. (b) Length-integrated population of levels 3 and 6 at time $t' = 2.45$ ps. For comparison $\int_0^l N_0 dz = 4.8 \times 10^{19}$ cm^{-2}. (c) Time-integrated ASE signal normalized to time-integrated input pump pulse signal.

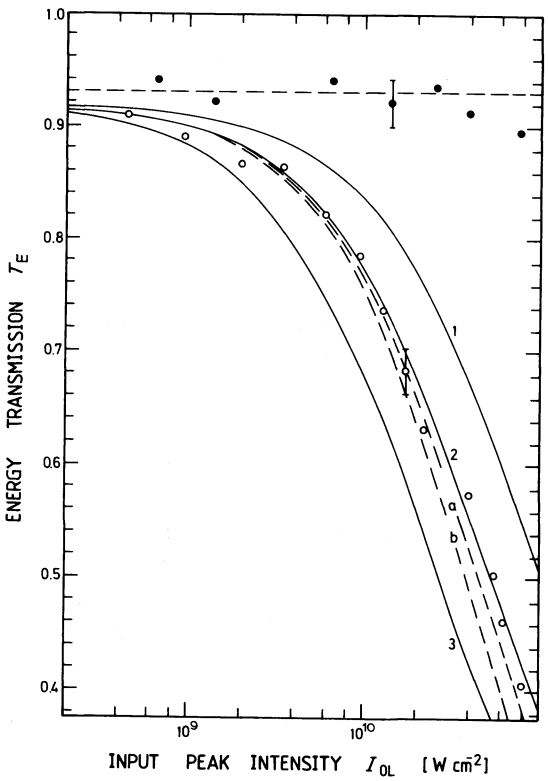

Figure 21 Energy transmission of laser light through PYC dissolved in HFIP. Data are listed in Table I. Cross-section spectra and fluorscence quantum distribution spectra are presented in [29]. The curves belong to: 1, $\sigma^{(2)} = 9 \times 10^{-50}$ cm^{4}s and $\sigma_{ex}^{L} = 0$; 2, $\sigma^{(2)} = 1.8 \times 10^{-49}$ cm^{4}s and $\sigma_{ex}^{L} = 0$; 3, $\sigma^{(2)} = 3.6 \times 10^{-49}$ cm^{4}s and $\sigma_{ex}^{L} = 0$; a, $\sigma^{(2)} = 1.8 \times 10^{-49}$ cm^{4}s and $\sigma_{ex}^{L} = 2 \times 10^{-18}$ cm^2; b, $\sigma^{(2)} = 1.8 \times 10^{-49}$ cm^{4}s and $\sigma_{ex}^{L} = 5 \times 10^{-18}$ cm^2.

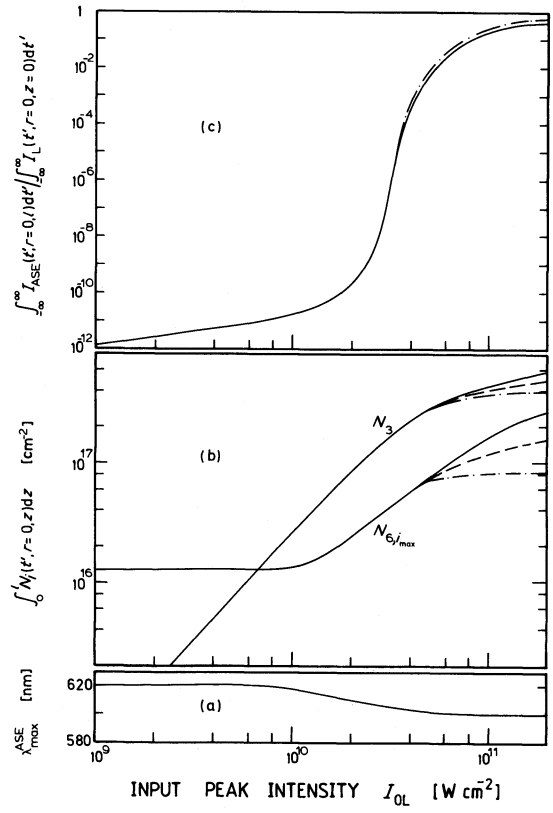

Figure 22 Characterization of two-photon induced amplified spontaneous emission of PYC dissolved in HFIP. Parameters are listed in Table I. Cross-section spectra are presented in [29]. (a) Wavelength of peak amplified spontaneous emission. (b) Length-integrated population of levels 3 and 6 at time $t' = 2.45$ ps. For comparison $\int_0^l N_0 dz = 6 \times 10^{19}$ cm^{-2}. (c) Time-integrated ASE signal normalized to time-integrated input pump pulse signal. Solid curves, $\tau_{v,6} = 4$ ps; broken curves, $\tau_{v,6} = 1$ ps; chain-broken curves, $\tau_{v,6} = 0.1$ ps.

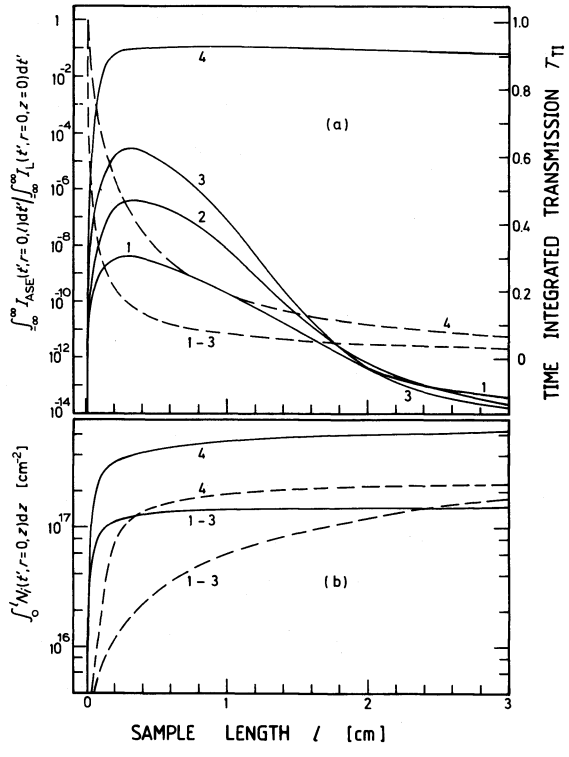

Figure 23 Influence of sample length on two-photon absorption dynamics. (a) Normalized time-integrated ASE signals (solid curves) and time-integrated transmissions (broken curves). (b) Length-integrated populations of level 3 (solid curves) and level 6 (broken curves). $I_{0L} = 10^{11}$ W cm^{-2}, $\varrho_6 = 5 \times 10^{-4}$, $e_{ASE} = 0.2$, $\sigma_{ex}^{ASE} = 0$. Other parameters belong to rhodamine 6G data on Table I. Curves 1–3, $\sigma^{(2)} = 10^{-49}$ cm^4 s and $\sigma_{ex}^{L} = 2 \times 10^{-17}$ cm^2 with $\sigma_{em}^{ASE} = 10^{-16}$ cm^2 (1), 1.5×10^{-16} cm^2 (2), and 2×10^{-16} cm^2 (3). Curve 4, $\sigma^{(2)} = 10^{-49}$ cm^4 s, $\sigma_{ex}^{L} = 0$, $\sigma_{em}^{ASE} = 1 \times 10^{-16}$ cm^2.

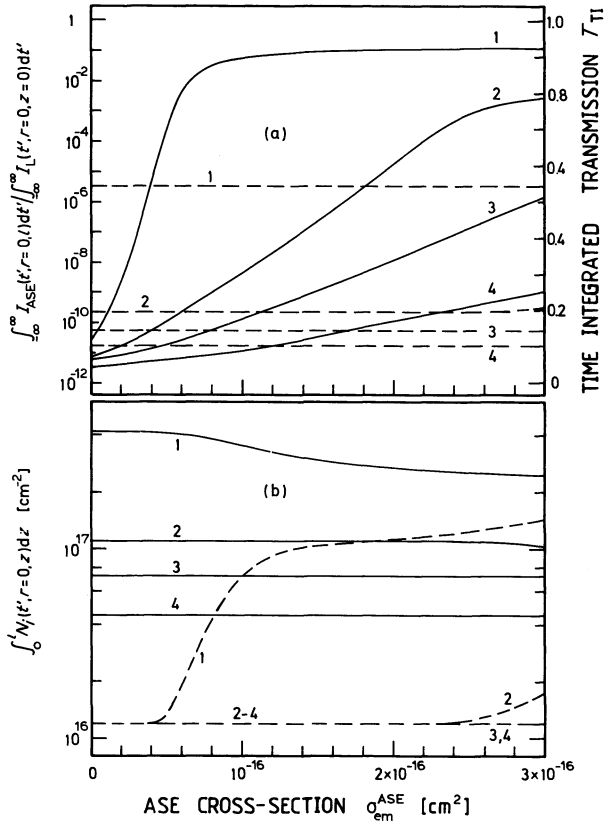

Figure 24 Influence of stimulated emission cross-section at frequency ν_{ASE} on two-photon absorption dynamics. (a) Normalized time-integrated ASE signals (solid curves) and time-integrated transmissions (broken curves). (b) Length-integrated populations of level 3 (solid curves) and level 6 (broken curves). $I_{0L} = 10^{11}\,W\,cm^{-2}$, $l = 0.2\,cm$, $\varrho_6 = 5 \times 10^{-4}$, $e_{ASE} = 0.2$, $\sigma^{(2)} = 1 \times 10^{-49}\,cm^4\,s$, $\sigma_{ex}^{ASE} = 0$. For other parameters, see rhodamine 6G data of Table I. Curves: 1, $\sigma_{ex}^{L} = 0$; 2, $\sigma_{ex}^{L} = 2 \times 10^{-17}\,cm^2$; 3, $\sigma_{ex}^{L} = 4 \times 10^{-17}\,cm^2$; and 4, $\sigma_{ex}^{L} = 8 \times 10^{-17}\,cm^2$.

The influence of the amplified spontaneous emission cross-section is shown in Fig. 24. The excited-state absorption cross-section σ_{ex}^{L} is changed for the various curves. The amplified spontaneous emission signal rises with σ_{em}^{ASE}. T_{TI} is only effected by σ_{em}^{ASE} if $\sigma_{ex}^{L} > 0$ and strong ASE generation occurs (slight indication by broken curve 2 of Fig. 24a). Rising σ_{ex}^{L}-values reduce the amplification of spontaneous emission since photons are lost for the population of level 3 (see N_3-curves of Fig. 24b). In case of strong amplified spontaneous emission (curves 1, $\sigma_{ex}^{L} = 0$) the upper ASE-level population N_3 reduces and the lower ASE-level population N_6 is filled. The transmitted laser pulse durations are independent of σ_{em}^{ASE}.

The influence of excited-state absorption σ_{ex}^{L} on T_{TI}, I_{ASE}, N_3, N_6 and $\Delta t_L(l)$ is depicted in Fig. 25. The two-photon absorption cross-section $\sigma^{(2)}$ is changed for the various curves. The effect of amplified spontaneous light generation is strongly reduced with rising σ_{ex}^{L} due to the reduced upper ASE level population N_3. Excess population of the lower ASE-level N_6 is present only at low σ_{ex}^{L}-values where amplification of spontaneous emission is efficient. The time-integrated transmission T_{TI} decreases with σ_{ex}^{L}. Only two curves for $\sigma^{(2)} = 8 \times 10^{-49}\,cm^4\,s$ (broken curve 1) and $\sigma^{(2)} = 2 \times 10^{-50}\,cm^4\,s$ (broken curve 5) are shown in Fig. 25a. The pulsewidth broadening by two-photon absorption is reduced by excited-state absorption. For high σ_{ex}^{L}-values even pulse shortening occurs, as is seen by the chain-broken curves in Fig. 25b (input pulse duration $\Delta t_L = 5\,ps$).

In the calculations to Figs 23 to 25 it was assumed that $\sigma_{ex}^{ASE} = 0$. An inclusion of the excited-state absorption of the fluorescence light does not change the depicted dependences of T_{TI} and $\Delta t_L(l)$, if σ_{em}^{ASE} is replaced by $\sigma_{em}^{ASE} - \sigma_{ex}^{ASE}$. A slight dependence of the normalized amplified spontaneous emission signal on σ_{ex}^{ASE} is observed for constant $\sigma_{em}^{ASE} - \sigma_{ex}^{ASE}$ as is shown in Fig. 26.

Output pulse shapes are presented in Fig. 27. Fig. 27a shows the shape of the transmitted pump pulse (broken curve) and of the amplified spontaneous emission pulse (solid curve) for $\sigma_{em}^{ASE} =$

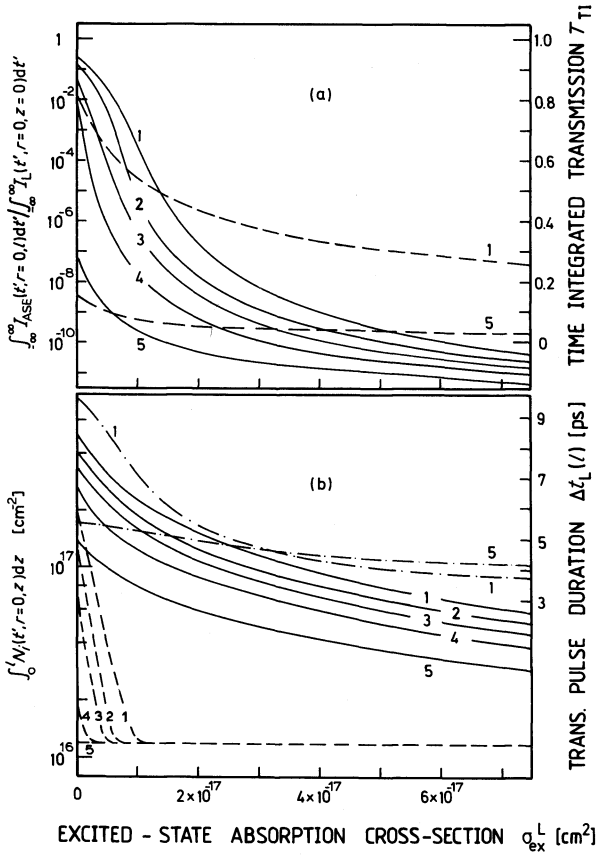

Figure 25 Influence of excited-state absorption of laser light on two-photon absorption dynamics. (a) Normalized time-integrated ASE signals (solid curves) and time-integrated transmissions (broken curves). (b) Length-integrated populations of level 3 (solid curves) and level 6 (broken curves), together with output pump pulse duration $\Delta t_L(l)$ (chain-broken curves). $I_{OL} = 10^{11}\,W\,cm^{-2}$, $l = 0.2\,cm$, $\varrho_6 = 5 \times 10^{-4}$, $e_{ASE} = 0.2$, $\sigma_{em}^{ASE} = 1 \times 10^{-16}\,cm^2$, $\sigma_{ex}^{ASE} = 0$, $\Delta t_L(0) = 5\,ps$. For other parameters, see rhodamine 6G data of Table I. Curves: 1, $\sigma^{(2)} = 8 \times 10^{-49}\,cm^4\,s$; 2, $\sigma^{(2)} = 2 \times 10^{-49}\,cm^4\,s$; 3, $\sigma^{(2)} = 1 \times 10^{-49}\,cm^4\,s$; 4, $\sigma^{(2)} = 5 \times 10^{-50}\,cm^4\,s$; 5, $\sigma^{(2)} = 2 \times 10^{-50}\,cm^4\,s$.

$10^{-16}\,cm^2$, $\sigma_{ex}^L = 0$, $I_{OL} = 10^{11}\,W\,cm^{-2}$ and $l = 2\,mm$ (for other parameters, see figure captions). The dotted curve indicates the input pump pulse shape. The pump pulse is broadened. The ASE pulse is strongly shortened (situation of strong amplified spontaneous emission). In Fig. 26b the situation of $\sigma_{em}^{ASE} = 10^{-16}\,cm^2$, $\sigma_{ex}^L = 4 \times 10^{-17}\,cm^2$, $I_{OL} = 10^{11}\,W\,cm^{-2}$ and $l = 2\,mm$ is depicted. The pump pulse is slightly shortened by the enhanced excited-state absorption at the trailing part (accumulation of population in level 3).

6. Conclusions

The S_0–S_1 two-photon absorption dynamics of some dyes has been investigated. The two-photon absorption cross-section, $\sigma^{(2)}$, and the excited-state absorption cross-section, σ_{ex}^L, may be determined by measurement of the energy transmission versus input pulse intensity without consideration of amplified spontaneous emission if amplified spontaneous emission does not remarkably change the S_1-level population. The occurrence of effective amplified spontaneous emission light generation is easily checked by forward fluorescence light detection. In the case of ASE-light generation with a conversion efficiency above 10^{-2} the depopulation of the S_1-state reduces the transmission loss by excited-state absorption. In this case the generation of amplified spontaneous emission light has to be included in the determination of $\sigma^{(2)}$ and σ_{ex}^L.

The amplification of fluorescence light of two-photon excited dye solutions may be applied to generate intense picosecond light pulses at new frequencies. In some cases this generation scheme may be an alternative to the generation of intense picosecond light pulses by single-photon excited amplified spontaneous emission [40, 45, 46] with frequency doubled pump pulses. It may be advantageous if excited-state absorption of second harmonic light hinders large excitation depths.

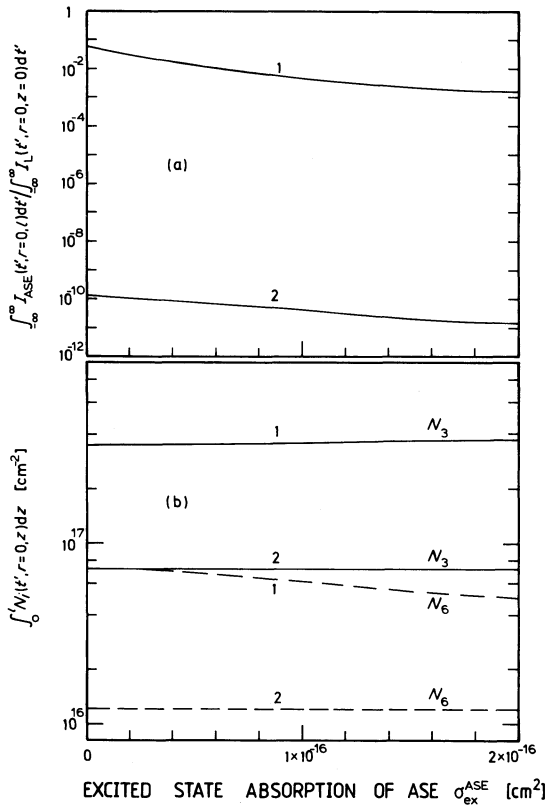

Figure 26 Influence of excited-state absorption cross-section σ_{ex}^{ASE} on amplified spontaneous emission. $\sigma_{em}^{ASE} - \sigma_{ex}^{ASE} = 1 \times 10^{-16}\,cm^2$ is held constant. The fixed parameters are $I_{OL} = 10^{11}\,W\,cm^{-2}$, $\sigma^{(2)} = 1 \times 10^{-49}$ $cm^4\,s$, $l = 2\,mm$, $\varrho_6 = 5 \times 10^{-4}$, $e_{ASE} = 0.2$ and rhodamine 6G data of Table I. The varied parameters are $\sigma_{ex}^{L} = 0$ for curves 1 and $\sigma_{ex}^{L} = 4 \times 10^{-17}\,cm^2$ for curves 2.

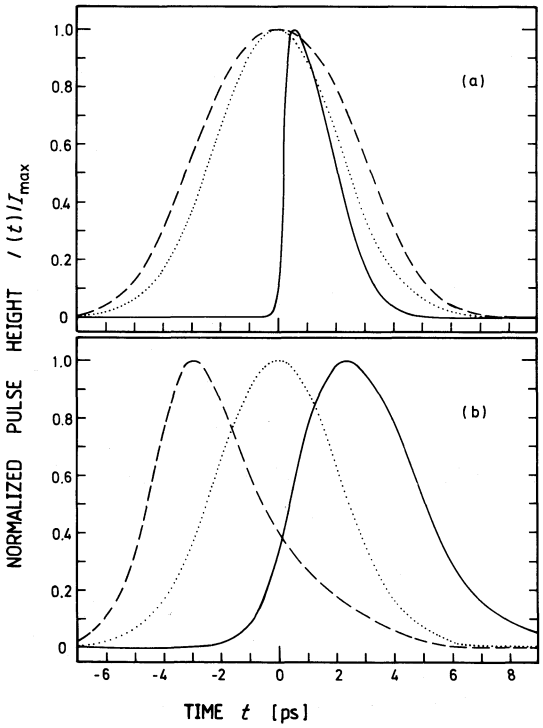

Figure 27 Pulse shapes. Dotted curves, input pump pulse; broken curves, output pump pulse; solid curves, amplified spontaneous emission pulse. (a) Two-photon absorption without excited-state absorption. Efficient amplified spontaneous emission. $I_{OL} = 10^{11}$ $W\,cm^{-2}$, $l = 0.2\,cm$, $\varrho_6 = 5 \times 10^{-4}$, $e_{ASE} = 0.2$, $\sigma^{(2)} = 1 \times 10^{-49}\,cm^4\,s$, $\sigma_{ex}^{L} = 0$, $\sigma_{em}^{ASE} = 1 \times 10^{-16}\,cm^2$, $\sigma_{ex}^{ASE} = 0$. (b) Two-photon absorption and strong excited-state absorption. Negligible amplified spontaneous emission. $I_{OL} = 10^{11}\,W\,cm^{-2}$, $l = 0.2\,cm$, $\varrho_6 = 5 \times 10^{-4}$, $e_{ASE} = 0.2$, $\sigma^{(2)} = 1 \times 10^{-49}\,cm^4\,s$, $\sigma_{ex}^{L} = 4 \times 10^{-17}\,cm^2$, $\sigma_{em}^{ASE} = 1 \times 10^{-16}\,cm^2$, $\sigma_{ex}^{ASE} = 0$. For other parameters, see rhodamine 6G data of Table I.

Acknowledgements

The authors are grateful to Dr U. Mayer (BASF) and Professor K. H. Drexhage for supply of the dye PYC. They thank the Deutsche Forschungsgemeinschaft for financial support and the Rechenzentrum of the University for provision of computer time.

References

1. J. A. GIORDMAINE, P. M. RENTZEPIS, S. L. SHAPIRO and K. W. WECHT, *Appl. Phys. Lett.* **11** (1967) 216.
2. W. RAPP and B. GRONAU, *Chem. Phys. Lett.* **8** (1971) 529.
3. A. N. RUBINOV, M. C. RICHARDSON, K. SALA and A. J. ALCOCK, *Appl. Phys. Lett.* **27** (1975) 358.
4. R. CUBEDDU, R. POLLONI, C. A. SACCHI and O. SVELTO, *IEEEE J. Quantum Electron.* **QE-5** (1969) 470.
5. J. M. RALSTON and R. K. CHANG, *Appl. Phys. Lett.* **15** (1969) 164.
6. E. W. VAN STRYLAND, H. VANHERZEELE, M. A. WOODALL, M. J. SOILEAU, A. L. SMIRL, G. GUHA and T. F. BOGGESS, *Opt. Engng* **24** (1985) 613.
7. J. F. REINTJES, 'Nonlinear Optical Parametric Processes in Liquids and Gases' (Academic Press, Orlando, 1984) Ch. 4.
8. P. P. BEY, J. F. GALBRAITH and H. RABIN, *IEEE J. Quantum Electron.* **QE-7** (1971) 86. J. C. DIELS and F. P. SCHÄFER, *Appl. Phys.* **5** (1974) 197. W. LEUPACHER and A. PENZKOFER (to be published).
9. F. P. SCHÄFER and W. SCHMIDT, *IEEE J. Quantum Electron.* **QE-2** (1966) 357.
10. D. J. BRADLEY, M. H. R. HUTCHINSON and H. KOETSER, *Proc. R. Soc.* **A329** (1972) 105.
11. J. P. HERMANN and J. DUCUING, *Opt. Commun.* **6** (1972) 105.
12. E. B. ASLANIDI and E. A. TIKHONOV, *Opt. Spectrosc.* **37** (1974) 446.
13. J. KRASINSKI, W. MAJEWSKI and M. GLÓDŻ, *Opt. Commun.* **14** (1975) 187.
14. B. FOUCAULT and J. P. HERMANN, *Opt. Commun.* **15** (1975) 412.
15. L. PARMA and N. OMENETTO, *Chem. Phys. Lett.* **54** (1978) 541.
16. P. SPERBER and A. PENZKOFER, *Opt. Quantum Electron.* **18** (1986) 381.
17. W. BLAU, W. DANKESREITER and A. PENZKOFER, *Chem. Phys.* **85** (1984) 473.
18. A. PENZKOFER and P. SPERBER, *ibid.* **88** (1984) 309.
19. A. PENZKOFER and W. FALKENSTEIN, *Opt. Quantum Electron.* **10** (1978) 399.
20. A. PENZKOFER, D. VON DER LINDE and A. LAUBEREAU, *Opt. Commun.* **4** (1972) 377.
21. TH. FÖRSTER, 'Fluoreszenz organischer Verbindungen (Vandenhoeck and Ruprecht, Göttingen, 1951).
22. TH. FÖRSTER and E. KÖNIG, *Z. Elekt.* **61** (1957) 344.
23. M. E. LAMM and D. M. LEVILLE, *J. Phys. Chem., Ithaca* **69** (1965) 3872.
24. C. A. PARKER, 'Photoluminescence of Solutions' (Elsevier, Amsterdam, 1968).
25. A. R. MONAHAN and D. F. BLOSSEY, *J. Phys. Chem., Ithaca* **74** (1970) 4014.
26. M. KASHA, in 'Spectroscopy of the Excited State', edited by B. DiBartolo (Plenum Press, New York, 1976) p. 337.
27. M. POPE and C. E. SWENBERG, 'Electronic Process in Organic Crystals' (Clarendon Press, Oxford, 1982).
28. Y. LU and A. PENZKOFER, *Chem. Phys.* **107** (1986) 175.
29. A. PENZKOFER, W. LEUPACHER, B. MEIER, B. RUNDE and K. H. DREXHAGE, *Chem. Phys.* **115** (1987) 143.
30. A. PENZKOFER and W. LEUPACHER, *J. Lumin.* **37** (1987) 61.
31. A. PENZKOFER and Y. LU, *Chem. Phys.* **103** (1986) 399.
32. J. B. BIRKS, 'Photophysics of Aromatic Molecules' (Wiley–Interscience, London, 1970) p. 301.
33. W. LEUPACHER, A. PENZKOFER, B. RUNDE and K. H. DREXHAGE, *Appl. Phys. B* **44** (1987).
34. S. J. STRICKLER and R. A. BERG, *J. Chem. Phys.* **37** (1962) 814.
35. J. B. BIRKS and D. J. DYSON, *Proc. R. Soc.* **A275** (1963) 135.
36. O. G. PETERSON, J. P. WEBB, W. C. McCOLGIN and J. H. EBERLY, *J. Appl. Phys.* **42** (1971) 1917.
37. N. N. VSEVOLODOV, L. P. KOSTIKOV, L. P. KAYUSHIN and V. I. GORBATENKOV, *Biophysics (GB)* **18** (1973) 807.
38. S. LI and C. Y. SHE, *Opt. Acta* **29** (1982) 281.
39. W. L. SMITH, in 'Handbook of Laser Science and Technology', vol. III, 'Optical Parameters: Part 1', edited by M. J. Weber (CRC Press, Boca Raton, Florida) p. 259.
40. P. SPERBER, M. WEIDNER and A. PENZKOFER, *Appl. Phys.* **B42** (1987) 185.
41. A. PENZKOFER, W. FALKENSTEIN and W. KAISER, *Chem. Phys. Lett.* **44** (1976) 82.
42. W. FALKENSTEIN, A. PENZKOFER and W. KAISER, *Opt. Commun.* **27** (1978) 151.
43. D. RICARD and J. DUCUING, *J. Chem. Phys.* **62** (1975) 3616.
44. J. WIEDMANN and A. PENZKOFER, *Nuovo Cimento* **63B** (1981) 459.
45. H. J. POLLAND, T. ELSAESSER, A. SEILMEIER and W. KAISER, *Appl. Phys.* **B32** (1983) 53.
46. ZS. BOT, S. SZATMÁRI and A. MÜLLER, *Appl. Phys.* **B32** (1983) 101.